LA-UR-81-433

MASTER

CONF-810620--1

TITLE: THE SUPPRESSION OF IGNITION BY INTERFACE INSTABILITIES IN SMALL FUSION TARGETS

AUTHOR(S): Ronald C. Kirkpatrick

SUBMITTED TO: 4th International Topical Conference on
High-Power Electron and Ion-Beam Research & Technology
June 29 - July 3, 1981, Palaiseau FRANCE

University of California

LOS ALAMOS SCIENTIFIC LABORATORY
Post Office Box 1663 Los Alamos, New Mexico 87545
An Affirmative Action/Equal Opportunity Employer

Form No. 836 R3
St. No. 2629
12/78

UNITED STATES
DEPARTMENT OF ENERGY
CONTRACT W-7405-ENG. 36

THE SUPPRESSION OF IGNITION BY INTERFACE INSTABILITIES IN SMALL FUSION TARGETS

by

R.C. Kirkpatrick
Los Alamos National Laboratory
Los Alamos, New Mexico 87545

ABSTRACT

Concern over hydrodynamic instabilities in small fusion targets has prompted numerous studies of instability onset, but few studies of the consequences. Here for the first time a mechanism is identified which tends to suppress ignition in small fusion targets. The mechanism is that of radiative energy loss into the increased area of a perturbed surface. Quantitative assessment of this mechanism is provided by modeling it in a 12 parameter burn code. It is contrasted with two other mechanisms and shown to be a significantly more serious consideration for DT ignition in the Wheeler mode.

1. INTRODUCTION

During the past few years several investigators have discussed hydrodynamic instabilities in laser and charged particle beam fusion targets. Among the numerical studies are the papers by Lindl and Mead [1] Fraley et al. [2], Toepfer and Tiffany [3], Henderson et al. [4] and McCrory et al. [5]. The major concern has been the loss of symmetry and outright breakup of the shell of material containing the DT plasma. Barnes [6] discussed additional possible adverse effects of instabilities and shock ejecta on DT ignition and reviewed the previous work of importance to this problem. Experimental work is being pursued by Assay, Toepfer, Perry, Widner and others at Sandia Laboratories [7], [8], [9], as well as elsewhere [10].

The reason for concern over instabilities is the degradation of target performance that logical extrapolation surely implies. However, a very important consequence of Rayleigh-Taylor instabilities (or any other surface distorting mechanism) has been previously overlooked. It arises through the coupling of the hydrodynamic instability to the radiative energy loss from the DT plasma. No previous numerical studies of small fusion targets have ever provided evidence of this coupling, nor is such a coupling easily demonstrated with the codes currently in use for design of small fusion targets. Unfortunately an almost total reliance on numerical simulation has long delayed the straight forward analysis which persuasively demonstrates the most important consequence of Rayleigh-Taylor and other hydrodynamic instabilities for inertial confinement fusion.

In the following sections I will describe the mechanism of increased energy loss into a Rayliegh-Taylor unstable surface and discuss the model used in the 12 parameter burn code. Then I will discuss some associated complications and survey the domain where it is expected to be a serious consideration. Finally, I will discuss the limitations imposed on small fusion targets designs.

2. THE MECHANISM

Whenever the interface between a DT plasma and the shell containing it is distorted, its area to volume ratio is increased. Distortion by instabilities such as Raleigh-Taylor (R-T) leaves the DT volume relatively unchanged, but as the limit of linear R-T growth is approached the distortion significantly increases the surface area. Since the energy loss rate into the confining shell is directly proportional to the area of the interface this has a direct consequence on the evolution of the DT plasma toward ignition.

2.1 The Area of a Rayleigh-Taylor Unstable Interface

In order to demonstrate the mechanism described above it is necessary to calculate the area of a distorted interface. Ideally one would like to integrate over 4π solid angle using some description of the distorted surface $R(\theta,\phi)$. However, for spherical harmonics (the obvious choice) the area is not integrable analytically. Also, there is no reason to believe the area for large amplitude x relative to the wavelength λ is accurately described by spherical harmonics and an accurate description is not really necessary to demonstrate the effect of the mechanism. For large mode numbers the distortions of a spherical surface are reasonably well approximated by those of a plane surface. An approximation which has a simple analytic form, yet is not so crude as to cast doubt on the results is that of pyramidal distortions for which the area of the surface is increased by a factor of

$$a_\lambda(x/\lambda) = \sqrt{1+(4x/\lambda)^2} \qquad (1)$$

over that of the undistorted plane surface.

For small amplitudes a_λ is quadratic in x/λ, as is that of a spherical cap of small height relative to its radius. While pyramidal distortions form a lower limit for a_λ due to smoother distortions, a stepped distortion of any complexity forms an upper limit. These upper and lower limits don't differ by more than 34%. Because large amplitude R-T growth is expected to develop spikes the pyramidal distortions will be assumed. This form of distortion will also allow later modification to account for additional complications. The area of the entire interface characterized by a single wavelength and a single amplitude would be

$$S(R,x/\lambda) = 4\pi R^2 a_\lambda(x/\lambda). \qquad (2)$$

2.2 Rayleigh-Taylor Growth

Plesset [11] has derived an expression for R-T growth which applies to a spherical interface between two immiscible incompressible fluids for which the outer fluid is infinite in extent, i.e. a thick shell approximation. His expression agrees with the thick shell limit for a more general result by Holm [12], and in the limit of zero surface tension reduces to

$$\ddot{x} + 3\dot{R}\dot{x}/R - Ax = 0, \tag{3}$$

where R is the mean radius of the interface, $\dot{R}$ its velocity, and A is given by

$$A = [n(n-1)\rho_2-(n+1)(n+2)\rho_1]\ddot{R}/[n\rho_2+(n+1)\rho_1]R, \tag{4}$$

where n is the mode number $2\pi R/\lambda$. In the limit of large n and large R this expression reduces to the product of the Atwood number and the acceleration divided by $\lambda=R/n$. It should be noted that finite initial values of either $\dot{x}$ or x may lead to unstable growth when A is positive and $\dot{R}$ is negative, as is the case during the compression phase of a small fusion target for all mode numbers

$$n>(\rho_2+3\rho_1)[1+(1+8\rho_1(\rho_2-\rho_1)/(\rho_2+3\rho_1)^2)^{1/2}]/2(\rho_2-\rho_1). \tag{5}$$

A phenomenon appropriately termed "fire polishing" has been previously described by Bodner [13] and further discussed by Cato [14] and others [4]. Tappert and Holm [15] made a simplified analysis of ablative stablization and arrived at a relation for the stabilizing pressure correct in the limit of a thick ablation layer. Reaccessment of that analysis leads to an additional term in equation (3) above, which includes the correction for finite ablation layer depth:

$$\ddot{x} + 3\dot{R}\dot{x}/R - Ax + Bx = 0, \qquad (6)$$

where the ablation coefficient B is

$$B = Q^{2/3}\rho_2^{1/3}\, f(\eta)(1-e^{-2\pi\eta L/R})2\pi\eta/RL(\rho_1+\rho_2)$$

$$= \gamma[(\gamma+1)Q/2\gamma]^{2/3}\rho_2^{1/3}\,(1-e^{-\eta L/R})\eta/RL(\rho_1+\rho_2). \qquad (7)$$

Here γ is the polytropic index for the ablated material, Q is the heat flux which drives the ablation wave, ρ_2 is the density ahead of the wave, L is the ablation layer depth, the function $f(\eta)$ is

$$f(\eta) = (1-\eta)^{1/3}\,\frac{\gamma\eta}{\gamma-1} - \frac{1}{2}\,(1-\eta)(1-\eta^2)^{-2/3}, \qquad (8)$$

and $\eta = \rho_1/\rho_2$ is the density ratio across the ablation front. Pollock [16] derived an expression for the flux Q due to radiation penetration which is correct in the limit of no hydrodynamic motion:

$$Q = \frac{8ac}{3\kappa_1\theta_1^n}\, c_{vs}/(n+5)\int_o^t \theta_r^{n+5}\, dt\,^{1/2}\,\theta_r^{n+5}, \qquad (9)$$

where a is the Stefan-Boltzman constant, c the speed of light, c_{vs} the specific heat of the ablated material, κ_1 the opacity at reference temperature θ_1, with $\kappa = \kappa(\theta_1/\theta_r)^n$, and θ_r is the radiation temperature.

Using the expression by Pollock for radiation penetration in terms of mass per unit area

$$x_o = \frac{n+5}{(n+4)^2}\,\frac{8ac}{3c_v\kappa_1\theta_1^n}\int_o^t \theta_r^{n+5}\, dt\,^{1/2}/\theta_r, \qquad (10)$$

the penetration depth is $L = x_o/\rho_1$, where density of the ablated material ρ_1 must be derived. If the internal energy of the ablated material is $e_1 = c_{vs}\theta_r - P_1\Delta\rho^{-1}$, and P_1 is the DT plasma pressure $(\gamma-1)\rho c_v\theta$, then

$$(\gamma_s-1)(c_{vs}\theta_r\rho_1-(\gamma-1)\rho c_v\theta(1-\frac{\rho_1}{\rho_2})) = (\gamma-1)\rho c_v\theta, \qquad (11)$$

so that

$$\rho_1 = \gamma_s(\gamma-1)\rho c_v\theta/(\gamma_s-1)(c_{vs}\theta_r+(\gamma-1)c_v\theta\rho/\rho_2) \qquad (12)$$

where ρ is the density of the DT plasma, γ is its ratio of specific heats, and θ is the DT material temperature. For the case $L<<\lambda$, the density profile $\rho(r)$ between R and R+L approximates a discontinuous jump from ρ to ρ_2 and this suggests a simplification to the treatment for evaluation of both the classical R-T coefficient A and the effect of "fire polishing". To evaluate A one may simply substitute ρ for ρ_1 in eq. (7). To account for the effect of "fire polishing" one may simply reduce the spike part of the area factor to properly allow for penetration to a depth x_o in the unpenetrated material ρ_2, and similarly reduce the "bubble" part of perturbed surface area. I have used the expressions

$$a_\lambda\left(\frac{x}{\lambda}\right) = (1+(4x/\lambda)^2)^{1/2}\left\{1-\left(\frac{2d}{\lambda}\right)^2\frac{(4x/\lambda)^2}{1+4(x/\lambda)^2}\left|1-2\frac{(1+(4x/\lambda)^2)^{1/2}-1}{(4x/\lambda)^2}\right|\right\} \qquad (13)$$

for $d < \frac{\lambda}{4}(1+(4x/\lambda)^2)^{1/2}/(4x/\lambda)$,

and $$a_\lambda(x/\lambda) = 2\left(\frac{4d}{\lambda}\right)^2\left|1-(1-(\lambda/4d)^2)^{1/2}\right| \qquad (14)$$

for $d > \frac{\lambda}{4}(1+(4x/\lambda)^2)^{1/2}/(4x/\lambda)$,

where $d = x_o/\rho_2$.

When the amplitude x exceeds the linear limit $\lambda/2$, then the equation for the R-T growth is taken to be

$$\ddot{x} = g\ddot{R} \tag{15}$$

For g = 0 there is no acceleration relative to the mean interface position R, while for g = 1, the tip of the R-T spike falls freely (constant velocity relative to the origin). No attempt has been made here to assess the correct value of g, but it is clear that $0 < g < 1$ bounds the physically reasonable value.

2.3 Added heat Capacity and Radiation Loss

The expression derived by Pollock and those which preceeded ([17], [18]) assumed slab geometry, but we need to correct for curvature of the ablating surface. For small penetration depth L relative to the curvature, it is only necessary to correct for the amount of penetrated material not included in the plane parallel penetration relation, hence for the added heat capacity of the material at the radiation temperature:

$$\Delta M = \int_0^{x_o} S(R,\tfrac{x}{\lambda})dx_o - S(R,\tfrac{x}{\lambda})x_o, \tag{16}$$

so that the heat capacity for radiation must be increased to

$$c_r' = (4a\theta_r^3 \tfrac{4\pi}{3} R^3 + c_{vR}\Delta M)/\tfrac{4\pi}{3} R^3. \tag{17}$$

In a previous paper Kirkpatrick [19] derived a relation for radiative loss into an opaque wall which was expressed in terms of the rate of change of the radiation temperature due to radiation loss $\dot{\theta}_{esc}$. To correct for the increased area of the perturbed interace $\dot{\theta}_{esc}$ need only be multiplied by $a_\lambda(\frac{x}{\lambda})$. To correct for the added heat capacity of material

at the radiation temperature, the rate for radiation temperature $\dot{\theta}_r$ must be reduced by the factor

$$\frac{c_r'}{c_r} = 1 + \frac{3\int_o^{x_o} R^2 a_\lambda dx_o}{4aR^3\theta_r^3} - \frac{3a_\lambda x_o}{4aR\theta_r^3} \quad . \tag{18}$$

3. THE CONSEQUENCES OF THE MECHANISM

In order to assess the importance of the mechanism outlined above, the equations set forth above have been incorporated in a twelve-parameter burn code [19]. This required the insertion of two additional parameters x and $\dot{x}$ plus their associated rate eqution, auxiliary relations. Obviously the consequences of the mechanism hinge on the initial values of $\dot{x}$ and x, and the importance of the mechanism must be judged in light of the reasonableness of the initial values and the magnitude of the effect.

3.1 An Example

For a target containing 837 μg of 50:50 DT and a 84 mg gold pusher with an initial internal energy of 121 J/mg, an initial implosion velocity of 110 μ/ns will provide ignition in the absence of initial perturbation of the DT/gold interface. However, failure results for an initial perturbation of about 3μ for a mode number n = 10. The failure is presented in Table 1. For much of the implosion x and $\dot{x}$ control the time step, and the reason is apparent in the last column which shows $a_\lambda(x/\lambda)$. The values of $a_\lambda(x/\lambda)$ do not represent a smooth variation. Instead, they reflect cyclic behavior due to the imbalance between A and B in equation (9). For constant coefficients equation (9) has oscilatory or exponential behavior depending on the sign of -A+B. Because -A+B > 0, x is oscilatory, but the amplitude of the oscilations grows exponentially if 3U/R is negative, a condition which is satisfied during the implosion (U<0). However, superimposed on

the growing amplitude of the oscilations is the penetration of radiation into the perturbed surface and this tends to reduce the effective area of the perturbed surface in accord with equation (16). Because x may be oscilatory, its value may be negative for the linear regime, but the area is increased for both positive and negative values of x. Beyond the linear limit $x>\lambda/2$, the amplitude of x is assumed to be monotonically increasing(g=0 in equation 15). This would result if an irreversible process such as Hemholtz instabilities disrupted the Taylor spike so that its tip became hydrodynamically decoupled from the remainder of the high density fluid [20]. The tip decelleration should be generally in accord with the theory developed for the flight of a meteor through the atmosphere [21], but no attempt has been made to follow the detailed physics past the linear limit of the R-T instability. Only one author [20] has attempted to quantify the highly nonlinear problem of large amplitude R-T growth and the subsequent Hemholtz instability. Clearly, more work is needed in this area. The value of $a_\lambda(x/\lambda)$ generated by the implosion presented in Table 1 is plotted in Figure 1.

3.2 A Survey

Figure 2 provides an overview of the effect of the perturbed surface on DT ignition. Here two regions of ignition [19] are shown in the (ρ_o, θ_o) plane. The initial conditions for this figure are the same as for the above example. The areas enclosed by the solid contours are the regions where ignition occurs in the absence of an initial perturbation, and those enclosed by the dashed contours are the regions where ignition occurs for an initial perturbation of 3.15 μ and n = 10. It is apparent that only ignition in the high gain (so called Wheeler) mode is threatened by the increased surface area that results from R-T instabilities. This is because radiation and material temperatures are nearly in equilibrium as the conditions necessary for ignition in the Wheeler mode are approached and energy is lost from the DT

volume mainly by radiation penetration into the material compressing the DT. However, in the other (hydrodynamic) mode of ignition energy is lost from the DT volume mainly by conduction which is little affected in the formulation presented here.

Figure 3 shows the same case in the (ρ_o, U_o) plane, where the assumption $\rho_o \alpha_o U^2$ has been made. The dashed line once again is for an initial perturbation of 3.15 μ with n = 10. Unfortunately it is the high gain mode that suffers from the surface perturbations.

3.3 Small Fusion Target Designs

Two obvious ways to avoid the problem created by initial perturbations in small fusion targets are (1)reduce the initial perturbations to a tolerable level, and (2)avoid the high gain mode. However, given current technology and the attractiveness of the high gain mode neither one of these options are acceptable. However, a third option may exist. That option involves a balance of the Taylor and ablative stablization terms in equation (9). If the oscilatory frequency of x can be made sufficiently small during the time that the convergence term is large, the value of x/λ may be kept sufficiently small to allow ignition. Additionally if the oscilatory frequency cannot be made small enough, there is still the possibility of adjusting the oscilatory frequency to make $a_\lambda(x/\lambda)$ small during the crucial interval when the material temperature is between about 1 keV and 2 keV.

It should be noted that no benefit is derived from "eliminating" the classical Taylor term by envoking "super" ablative stabilization as long as a strong convergence term like that derived by Plessett exists, since only a small improvement is achieved, i.e., the rms value of x/λ, $\sqrt{(x/\lambda)^2}$ still grows exponentially during implosion. However, Plessett's derivation correctly applies only to the incompressible case, and one might reasonably expect a reduction in the convergence term for the compressible case. Also, if the above discussion of the RT-growth assumes that the coefficients in the Plessett

equation are constant. Clearly, much more work is needed on the problem of hydrodynamic instabilities and their consequences.

4. ACKNOWLEDGEMENTS

I am indebted to the numerous authors who have studied the problem of Taylor instabilities and in particular to Darryl Holm who has provided assistance in the analysis of ablative stabilization and in understanding the behavior of equation (9).

References

1. J.D. Lindl and W.C. Mead, Phys. Rev. Letters 34 (1975) 1273

2. G. Fraley, W. Gula, D. Henderson, R. McCrory, , R. Malone, R. Mason, and R. Morse, Plasma Physics and Controlled Nuclear Fusion Research, paper IAEA-CN-33/F5-5, International Atomic Energy Agency, Vienna (1974).

3. A.J. Toepfer and W.J. Tiffany, Bull. Am. Phys. Soc. 23 (1978) 96.

4. D.B. Henderson, R.L. McCrory, and R.L. Morse, Phys. Rev. Letters 33 (1974) 205.

5. R.L.. McCrory, R.L. Morse, and K.A. Taggart, Nucl. Science and Eng. 64 (1977) 1.3 .

6. J.F. Barnes, Bull. Am. Phys. Sec. 23 (1978) 95.

7. J.R. Assay, and L.D. Bertholf, Bull. Am. Phys. Soc. 23 (1978) 95 and SAND 78-1256.

8. L.P. Mix, F.C. Perry, A.J. Toepfer, and M.W. Widner, Bull. Am. Phys. Soc. 23 (1978) 96.

9. F.C. Perry, L.P. Mix, and A.J. Toepfer, Bull. Am. Phys. Soc. 23 96 (1978).

10. J.W. Hopson and B.W. Olinger, Bull. Am. Phys. Soc. 23, (1978) 95.

11. M.S. Plessett, Journal of Appl. Phys. 25,(1954) 96.

12. D.D. Holm, private communication.

13. S.E. Bodner, Phys. Rev. Letters 33 (1974) 761.

14. P.J. Cato, Phys. Fluids 21 (1978) 30.

15. F.D. Tappert and D.D. Holm, "Fire-Polishing Stabilization", an internal Los Alamos Scientific Laboratory memo (1976).

16. R. Pollock, "Radiation Penetration Under Monotone Increasing Boundary Temperature", unpublished (1971).

17. R.E. Marshak, Phys. Fluids 1 (1958) 1.

18. A.G. Petschek, R.E. Williamson, J.K. Wooten, The Penetration of Radiation with Constant Driving Temperature, Los Alamos Scientific Laboratory Rept. LAMS-2421 (1960).

19. R.C. Kirkpatrick, Nuclear Fusion 19 (1979) 69.

20. E.N. Cappriotti, Ap. J. 179 (1973) 495.

21. E.J. Opik, Physics of Meteor Flight in the Atmosphere (Interscience Tracts on Physics and Astronomy #6), Interscience (1958).

TABLE 1.

CYC	T	R	U	C	θ_e	θ_i	θ_r		
0	0.	0.06300	-0.11000	0.8000	0.07	0.07	0.07	0.	0
0	0.	-0.	0.50000	0.50000	-0.	0.	-0.		
1	0.000	0.06299	-0.11000	0.8002	0.07	0.07	0.07	0.0000	-3
DPEN;TAYL=		1.74E-06	3.15E-04	3.71E-08	1.21E+00	3.18E-05	1.91E-06		
		4.32E-03	1.45E-05	6.88E-04	1.55E-03	3.54E-05			
10	0.006	0.06231	-0.10996	0.8269	0.07	0.07	0.07	0.0000	13
DPEN;TAYL=		2.71E-06	3.15E-04	5.41E-06	1.21E+00	5.06E-05	3.03E-06		
		4.57E-03	3.23E-05	5.68E-04	1.36E-03	3.69E-05			
20	0.124	0.04939	-0.10884	1.6603	0.11	0.11	0.11	0.0000	3
DPEN;TAYL=		1.24E-05	3.29E-04	2.92E-04	1.27E+00	3.68E-04	1.79E-05		
		1.46E-02	7.85E-05	1.56E-03	3.66E-03	1.12E-04			
30	0.246	0.03626	-0.10623	4.1959	0.21	0.21	0.21	0.0000	3
DPEN;TAYL=		3.71E-05	4.03E-04	9.14E-04	1.42E+00	2.05E-03	6.53E-05		
		6.85E-02	7.55E-04	1.07E-02	2.11E-02	6.31E-04			
40	0.310	0.02957	-0.10330	7.7354	0.32	0.32	0.31	0.0000	14
DPEN;TAYL=		7.44E-05	4.49E-04	9.37E-05	1.53E+00	6.18E-03	1.46E-04		
		1.88E-01	3.25E-03	3.69E-02	6.55E-02	2.02E-03			
50	0.336	0.02687	-0.10142	10.3119	0.38	0.38	0.37	0.0000	14
DPEN;TAYL=		1.02E-04	4.31E-04	-1.73E-03	1.52E+00	1.03E-02	2.08E-04		
		3.00E-01	6.30E-03	6.49E-02	1.10E-01	3.10E-03			
60	0.367	0.02383	-0.09844	14.7747	0.47	0.47	0.47	0.0000	14
DPEN;TAYL=		1.50E-04	3.15E-04	-6.48E-03	1.36E+00	1.92E-02	3.13E-04		
		5.37E-01	1.40E-02	1.29E-01	2.07E-01	3.98E-03			
70	0.417	0.01902	-0.09014	29.0516	0.70	0.70	0.69	0.0000	14
DPEN;TAYL=		2.98E-04	-2.90E-04	-1.44E-02	1.34E+00	5.98E-02	5.75E-04		
		1.57E+00	5.77E-02	4.36E-01	6.48E-01	-1.07E-02			
80	0.434	0.01755	-0.08594	36.9692	0.80	0.80	0.78	0.0000	14
DPEN;TAYL=		3.74E-04	-4.71E-04	-5.45E-03	1.56E+00	8.82E-02	7.48E-04		
		2.27E+00	9.10E-02	6.50E-01	9.48E-01	-2.61E-02			
90	0.440	0.01709	-0.08435	40.0496	0.83	0.83	0.82	0.0000	14
DPEN;TAYL=		4.03E-04	-4.86E-04	-5.79E-06	1.59E+00	1.00E-01	8.18E-04		
		2.57E+00	1.05E-01	7.38E-01	1.07E+00	-3.08E-02			
100	0.444	0.01668	-0.08280	43.0758	0.86	0.86	0.85	0.0000	14
DPEN;TAYL=		4.30E-04	-4.72E-04	5.92E-03	1.57E+00	1.12E-01	8.87E-04		
		2.86E+00	1.20E-01	8.27E-01	1.19E+00	-3.32E-02			
110	0.463	0.01519	-0.07578	57.0648	0.99	0.99	0.97	0.0000	14
DPEN;TAYL=		5.48E-04	-1.21E-04	3.04E-02	1.15E+00	1.73E-01	1.16E-03		
		4.36E+00	1.92E-01	1.26E+00	1.80E+00	-1.28E-02			
120	0.483	0.01376	-0.06594	76.7422	1.14	1.14	1.12	0.0000	14
DPEN;TAYL=		7.05E-04	4.94E-04	2.00E-02	1.60E+00	2.70E-01	1.48E-03		
		6.75E+00	3.08E-01	1.93E+00	2.73E+00	8.37E-02			
130	0.490	0.01336	-0.06230	83.8377	1.19	1.19	1.17	0.0000	14
DPEN;TAYL=		7.60E-04	5.68E-04	2.98E-03	1.69E+00	3.09E-01	1.63E-03		
		7.67E+00	3.50E-01	2.17E+00	3.08E+00	1.11E-01			
140	0.491	0.01324	-0.06113	86.0881	1.20	1.20	1.18	0.0000	14
DPEN;TAYL=		7.77E-04	5.68E-04	-3.12E-03	1.69E+00	3.22E-01	1.68E-03		
		7.98E+00	3.64E-01	2.25E+00	3.19E+00	1.16E-01			
150	0.501	0.01269	-0.05477	97.9360	1.27	1.27	1.25	0.0000	14
DPEN;TAYL=		8.70E-04	3.83E-04	-3.50E-02	1.46E+00	3.92E-01	1.92E-03		
		9.62E+00	4.37E-01	2.67E+00	3.78E+00	9.36E-02			
160	0.519	0.01184	-0.04118	120.3572	1.41	1.41	1.39	0.0001	14
DPEN;TAYL=		1.07E-03	-4.37E-04	-4.13E-02	1.49E+00	5.52E-01	2.30E-03		
		1.31E+01	6.10E-01	3.59E+00	5.07E+00	-1.46E-01			
AT LINEAR LIMIT!									
WLIM	TAYL	UWL	RAYL	ATWOOD	TAYV				
5.83E-04	5.93E-04	2.44E-03	1.17E-02	0.	2.36E-02				
170	0.539	0.01119	-0.02212	142.6137	1.57	1.57	1.54	0.0002	14
DPEN;TAYL=		1.38E-03	9.64E-04	2.36E-02	1.57E+00	7.99E-01	2.95E-03		
		1.72E+01	8.36E-01	4.73E+00	6.58E+00	4.08E-01			
TAYL	TAYV	UWL	XPEN						
1.50E-03	2.36E-02	3.78E-03	1.90E-03						
172	0.561	0.01096	0.00173	151.9918	1.73	1.73	1.69	0.0004	5
DPEN;TAYL=		1.[illegible]E-03	1.50E-03	2.36E-02	1.47E+00	1.15E+00	3.78E-03		
		2.02E+01	1.11E+00	5.89E+00	7.93E+00	7.16E-01			
182	0.653	0.01518	0.08014	56.9108	1.39	1.39	[illegible]		

FIGURE 1

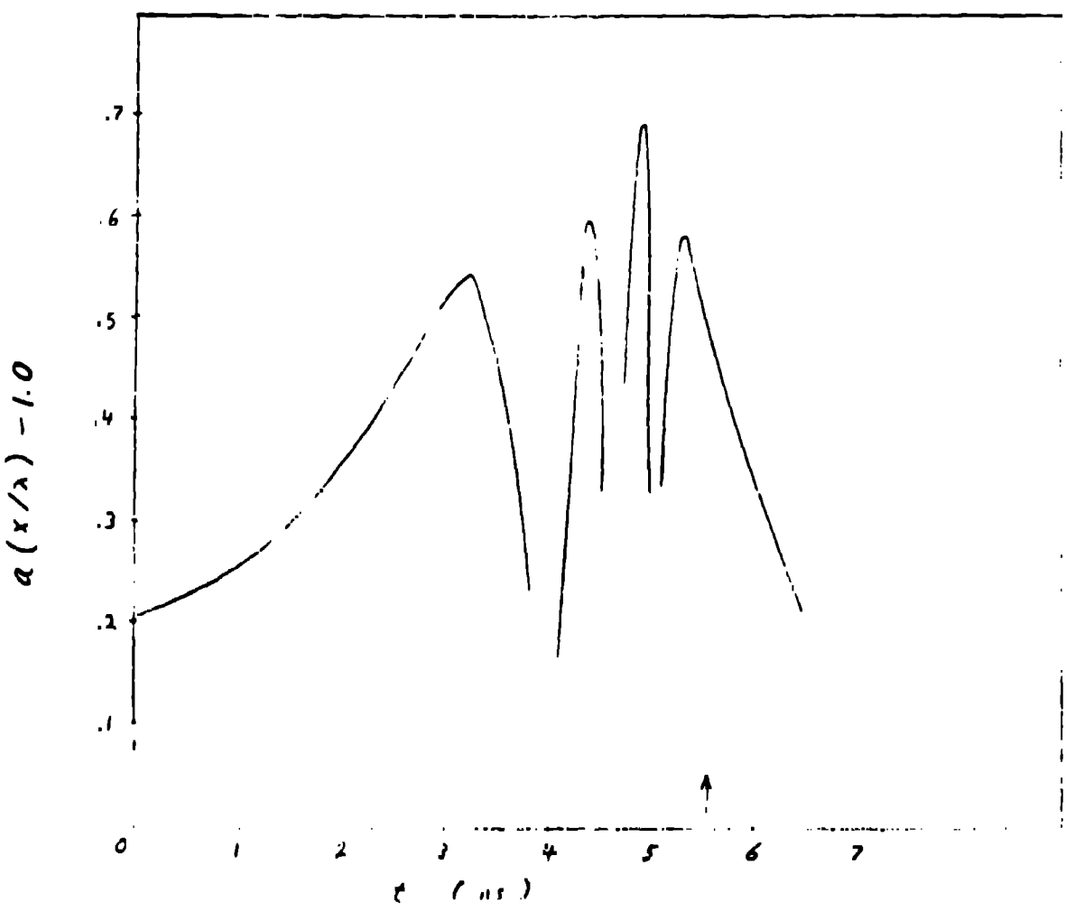

Time dependence of the area factor $a(x/\lambda)$. Note the repeated rise and fall due to the oscilatory nature of the instability amplitude. The arrow marks the pusher turn-around time.

FIGURE 2

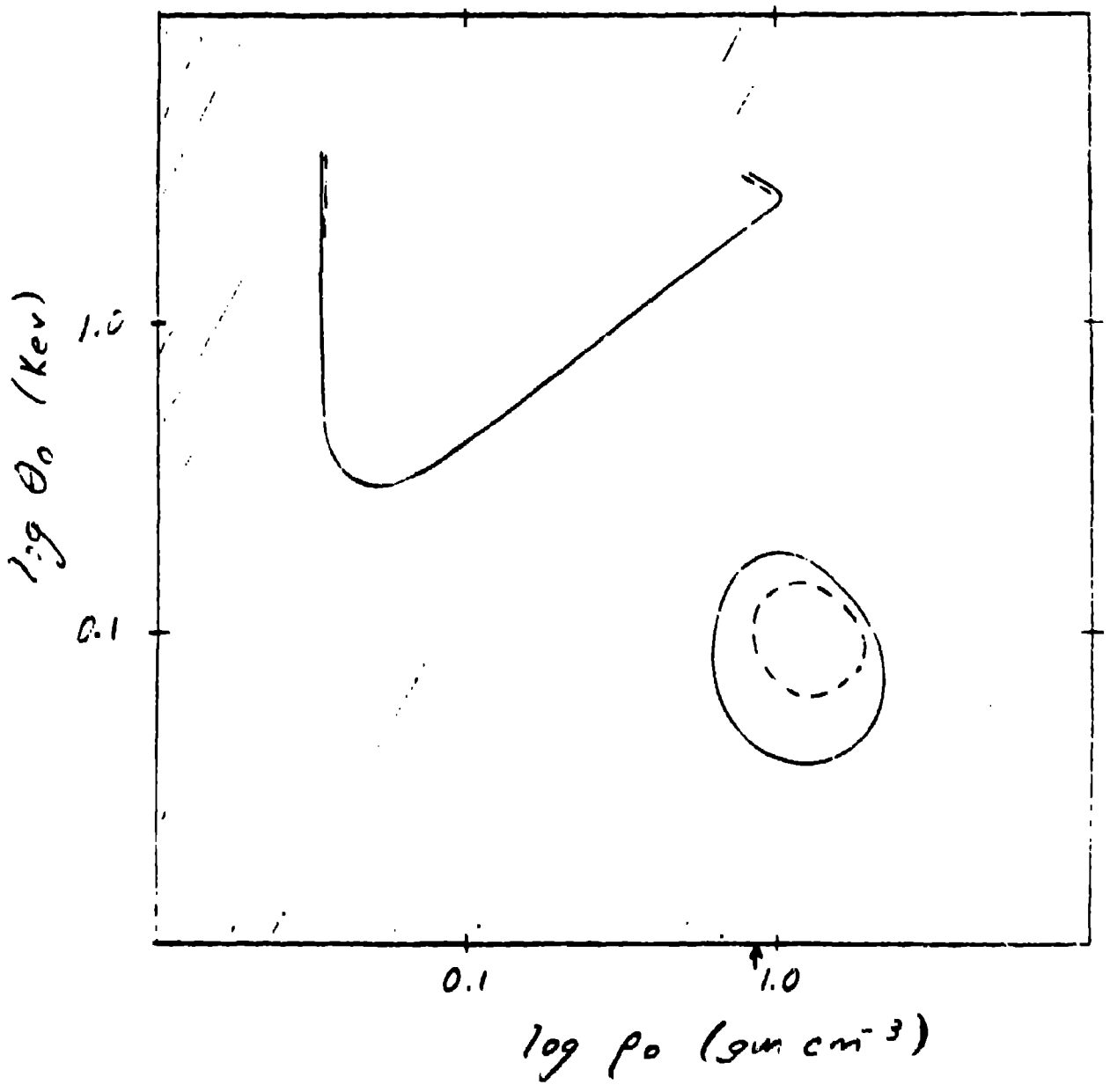

An overview of the effect of the perturbed surface on DT ignition. The solid contours delineate the ignition regions for no initial perturbation - hence no instability growth, while the dashed contours show the change when the initial perturbation is $x = 3.15\mu$ with a mode number of $n = 10$. Only the high gain mode of ignition at low θ_0 and high ρ_0 is significantly affected by the instability growth.

FIGURE 3

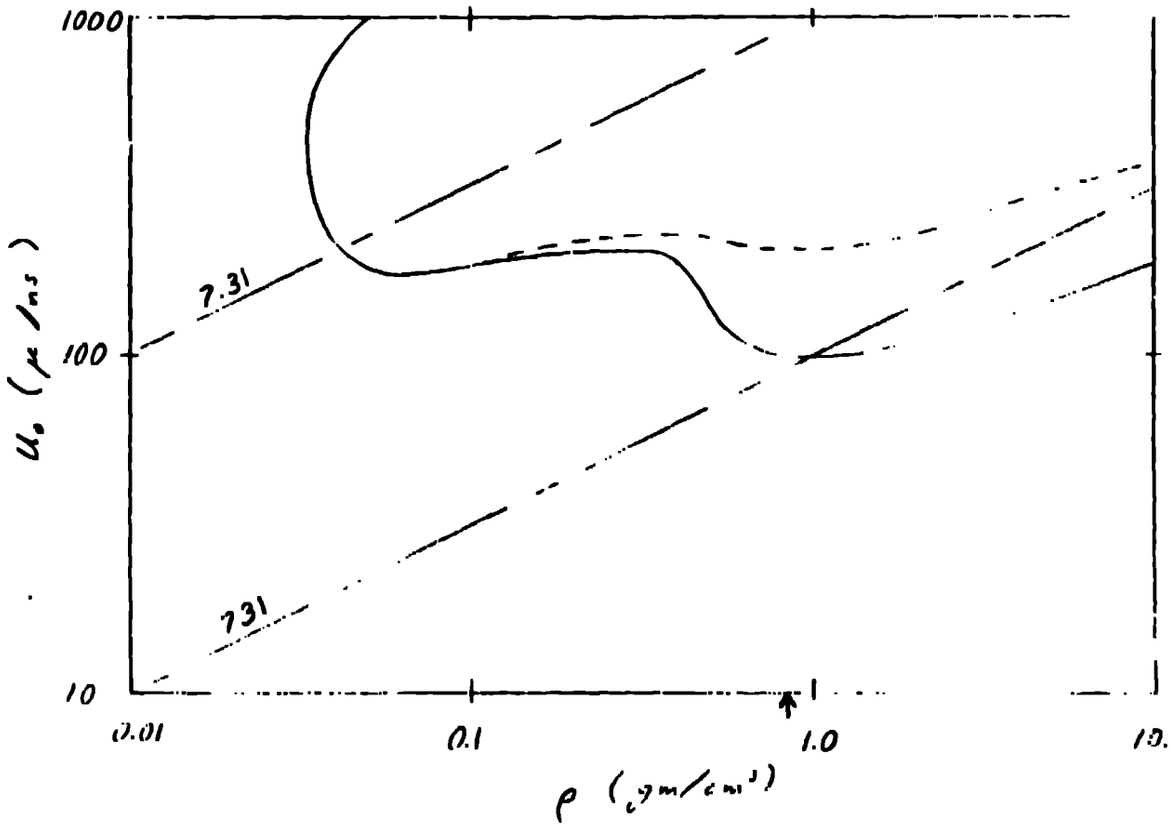

An overview in the (ρ_o, U_o) plane with $\theta_o \approx U_o^2$. The dashed curve is for the same perturbation as in Figure 2. The two dot-dash diagonal lines are lines of constant maximum theoretical gain ($2EM_{DT}/M_{SH}U_o^2$). The arrow marks liquid density DT (19), the physical limit on initial density.